Sudipta Das · N. Anveshkumar ·
Joydeep Dutta · Arindam Biswas *Editors*

Advances in Terahertz Technology and Its Applications

Springer

Advances in Terahertz Technology and Its Applications

Sudipta Das · N. Anveshkumar · Joydeep Dutta ·
Arindam Biswas
Editors

Advances in Terahertz Technology and Its Applications

Springer

Editors
Sudipta Das
Department of Electronics
and Communication Engineering
IMPS College of Engineering
and Technlogy
Malda, West Bengal, India

Joydeep Dutta
Department of Computer Science
Kazi Nazrul University
Asansol, West Bengal, India

N. Anveshkumar
Department of Electronics
and Communication Engineering
VIT Bhopal University
Bhopal, Madhya Pradesh, India

Arindam Biswas
Department of Computer Science
School of Mines and Metallurgy
Kazi Nazrul University
Asansol, West Bengal, India

ISBN 978-981-16-5730-6 ISBN 978-981-16-5731-3 (eBook)
https://doi.org/10.1007/978-981-16-5731-3

This Springer imprint is published by the registered company Springer Nature Singapore Pte Ltd.
The registered company address is: 152 Beach Road, #21-01/04 Gateway East, Singapore 189721, Singapore

Preface

In these modern times, the growing applications in communication, sensing, security, safety, spectroscopy, manufacturing, biomedical, agriculture, imaging, etc., demand for higher resolution, greater speeds, and wider bandwidth support. Thanks to THz technology that makes it possible due to its enormous advantages like non-ionizing signal nature, compactness, higher resolution, spatial directivity, high-speed communication, and greater bandwidth. Since the THz radiation covers frequencies from 0.1 THz to around 10 THz and is highly attenuated by atmospheric gases, it is mainly used in short-distance applications.

This book is aimed to bring the emerging application aspects of THz technology and various modules used for its successful realization. It gathers scientific technological novelties and advancements already developed or under development in the academic and research communities. This work focuses on recent advances and different research issues in terahertz technology and would also seek out theoretical, methodological, well-established, and validated empirical work dealing with these different topics. The chapters cover a very vast audience from basic science to engineering, technology experts, and learners. This could eventually work as a textbook for engineering and communication technology students or science master's programs and for researchers as well. These chapters also serve the common public interest by presenting new methods for application areas of technology, its working, and its effect on the environment and human health, etc.

In particular, this textbook covers the broad categories of THz technology aspects, advantages, disadvantages, applications, communication trends, challenges and security, various modules like antennas and absorbers under different material considerations, solid-state devices, THz generators, realization of optical NOT and NAND gates, de-multiplexers and parity generator, THz e-healthcare system, THz metasurface, oversampled OFDM modulation technique in THz communication systems. The antenna trends include planar antennas, horn geometries, SIW structures, THz arrays, fabrication techniques, etc. The solid-state devices cover wide bandgap semiconductors, IMAPTT diodes, etc.

Once the readers finish the study of this book, then definitely they will get to know about the importance of THz technology, advancement in the field, applications,

THz modules, and future scope. It also leads to enhancement in their knowledge in THz technology and gives a platform to future technology and novel application realization.

Malda, West Bengal, India — Sudipta Das
Bhopal, Madhya Pradesh, India — N. Anveshkumar
Asansol, West Bengal, India — Joydeep Dutta
Asansol, West Bengal, India — Arindam Biswas

Contents

About the Editors

Dr. Sudipta Das obtained his Ph.D. degree from the University of Kalyani, India. He is currently working as Associate Professor in the Department of Electronics and Communication Engineering at IMPS College of Engineering & Technology, West Bengal, India. He is having 10 years of teaching and 7 years of research experiences. His research interests are microstrip antennas for microwave, mm-wave and THz communication systems, flexible antenna design, filter design, FSS, RFID, microwave components, and THz systems.

Dr. N. Anveshkumar is currently working as Assistant Professor in the Department of ECE, VIT Bhopal University, Bhopal, India. He pursued his doctoral degree from VNIT Nagpur, in 2019 under the guidance of Dr. A. S. Gandhi from the field of antennas, RF circuits, and wireless communications. He is having 2 years of teaching and research experience. Till now, he published his research papers in seven SCI Journals, two Scopus Indexed Journals, five international journals and 11 in international and national conferences. His research interests include antennas, RF circuits, wireless communications, and embedded systems. Currently, he is working in the area of high directional UWB antennas, reconfigurable antennas, cognitive radio antennas, RF energy harvesting, THz antennas, and mobile antennas.

Dr. Joydeep Dutta completed his Ph.D. from the Department of Computer Science and Engineering, NIT Durgapur, in 2020. He has more than 9 years of teaching experience and 2 years of industrial experience. His current research interests include network optimization problems, artificial intelligence, evolutionary algorithms, combinatorial optimization, etc.

Dr. Arindam Biswas received his M.Tech. in radio physics and electronics from the University of Calcutta, India, in 2010, and Ph.D. from NIT Durgapur, in 2013. He was Postdoctoral Researcher at Pusan National University, South Korea, under the prestigious BK21PLUS Fellowship. He was Visiting Professor at Research Institute of Electronics, Shizuoka University, Japan. Currently, he is working as Associate Professor in the School of Mines and Metallurgy, Kazi Nazrul University, Asansol, West Bengal, India. His research interests are in the areas of carrier transport in low-dimensional systems and electronic devices, nonlinear optical communications, and THz semiconductor sources.

Recent Trends in Terahertz Antenna Development Implementing Planar Geometries

V. Adhikar, A. Karmakar, B. Biswas, and C. Saha

Abstract This chapter summarizes design and development of antenna using microfabrication technology for Terahertz application. Two different types of antennas have been discussed here with fabrication process details along with design strategies. Effect of imbibed process related imperfections on final device performance are highlighted here with the help of mathematical models. Surface roughness becomes a bottleneck for realizing any device in THz-regime, which has been explained with various analytical models. FEM-based 3D simulator is used extensively for analyzing all designs. Parametric simulations were carried out to get the optimized design values. The first design is complete of planar type. It is based on a flexible microwave substrate named LCP (Liquid Crystal Polymer), which is very thin (~100 μm), hardly moisture absorbent (<0.04%), and moreover bio-compatible in nature. A 100 GHz design specification is chosen for the targeted medical imaging antenna array structure offers a directive gain of around 19.3 dBi. Electrical equivalent circuit modeling of the whole array structure is also chalked out in this chapter, which eases to understand the interaction between various radiating elements with adjacent parasitic counterparts. Second portion of the chapter introduces design and simulation of a silicon micro-machined W-band sectoral H-plane horn antenna with proposed fabrication process details. Selection of design parameters has been summarized with the help of analytical models and parametric simulations in a 3D-EM environment. Proposed design offers around 13 dBi gains.

Keywords THz antenna · Circuit modeling · LCP · Sectoral horn · Superstrate

V. Adhikar
COMSOL Multi Physics Software Limited, Bengaluru, India

A. Karmakar (✉)
Semi-Conductor Laboratory (SCL), Department of Space, Government of India, Chandigarh, India

B. Biswas
Indian Institute of Science Education and Research (IISER), Mohali, Chandigarh, India

C. Saha
Indian Institute of Science and Technology (IIST), Trivandrum, India

S. Das et al. (eds.), *Advances in Terahertz Technology and Its Applications*,
https://doi.org/10.1007/978-981-16-5731-3_1

1 Introduction

In the recent era, remarkable research interests are being paid to the Terahertz (THz) band (0.1 to 10 THz) in various applications for wireless communication sectors, medical diagnostics, radio astronomy, imaging, and many other instrumentation circuits because of its several unique features including free-license wide spectral bandwidth, high spectral resolution, non-ionization property, tranquil from EMI/EMC issue, etc. [1–6]. However, like other technology it has also some demerits in context with high path-loss factors and attenuation in the presence of water vapor or hydroxyl ions. To eradicate these issues, high gain antennas are inevitable for effective establishment of communication links between the transmitter and receiver. Simultaneously, several atmospheric windows co-exist across the THz frequency spectrum, where the path-loss factors are reduced significantly [7]. THz-communication can be established at these low loss frequencies to enhance the wireless link reliability factor. On the contrarily, since the dimension of wavelength becomes very short (0.03 to 3 mm) at THz frequencies, manufacturing antenna at this frequency band becomes a challenging task while employing cost-effective standard fabrication processes. Furthermore, the integration of the antenna with other building blocks of communication sub-system plays a pivotal role to attain the overall figure of merit.

This chapter demonstrates the design and development of two different types of THz-antennas implementing planar geometries. The antennas are based on standard micro-fabrication technologies. One of the antennas is relied upon silicon micromachining process, whereas the other candidate is focused on organic type microwave substrate called 'Liquid Crystal Polymer (LCP)'. Simple design with enriched performance is the attractive feature of the present structures. In the present chapter, the detailed design, simulation, effect of various design parameters, fabrication process intricacies, and finally the developed architectures have been demonstrated for two specified antenna types. Finally, the electrical equivalent circuit modeling aspects are also briefly touched upon for a better understanding of the device physics in association with various parasitic effects.

2 Designing of THz Antenna

Antenna being the electronic eye of whole communication system, its design is always an exigent task to an RF/antenna engineer. For the THz frequency, some more additional constraints act as supplementary with the generic requirements. In this section, the design aspects of two different types of THz antenna are discussed in detail.

2.1 Microstrip Patch Antenna Array

As compared to other antenna candidates for THz frequency ranges, fortunately, microstrip patch antenna inherits potential capabilities to satisfy mandatory requirements of link establishment. In this sub-section, series-fed rectangular shaped microstrip patch antenna (RMAA) array design is discussed. Ease of design and fabrication suitability with a cost-effective way is the attractive feature of this antenna module. As previously discussed in the introduction part, due to higher atmospheric attenuation at the THz frequency range, high gain antennas are essential for THz technology. Herein, the gain for RMAA is enhanced up to 19 dBi either by introducing parasitic elements or by appending the superstrate layer. LCP has been used as a base substrate material for the antenna design. It is a non-toxic, bio-compatible substrate with a permittivity value of 3.14 and dielectric loss tangent of around 0.002 [8]. It is a kind of organic polymer. Surface-wave and leaky wave problems are inherently eliminated/suppressed at higher frequency ranges for this substrate, which is usually of 4 mil (~100 μm) thickness and of flexible in nature. It can be wrapped over outside of any 3D cylindrical/circular shaped object. Conformal design can be made comfortably out of this, which is desirable for several bio-medical usages and air-borne applications [9, 10], targeting for THz frequency regime.

Proposed antenna structure comprises series-fed five patch elements, each having length *'L'* and width *'W'* and loaded with parasitic patch elements of length and width *'L'* and *'W_p'* on both sides of non-radiating edges of the five elements. Figure 1 shows the schematic of the proposed antenna. Dimension of the patch width *'W'* and length *'L'* is evaluated using Eq. (1) and (2) [11] and given by,

$$W = \frac{c}{2f_r}\sqrt{\frac{2}{1+\epsilon_r}} \tag{1}$$

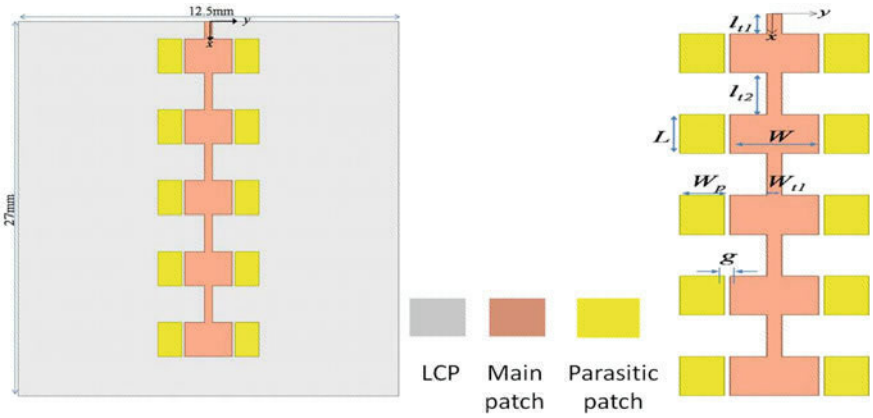

Fig. 1 Top view and dimensions of microstrip patch array with parasitic patches

$$L = \frac{c}{2f_r\sqrt{\epsilon_{eff}}} - 2\Delta L \tag{2}$$

where, ϵ_{eff} is an effective dielectric constant, and 'ΔL' is extended length on both sides of the radiating patch due to the fringing field [11]. Segments of the transmission line in between the patches are responsible for phase matching. The dimension of these transmission lines, i.e., length 'l_{t1}' and 'l_{t2}' and width 'W_{t1}', are computed as follows [12]

$$l_{t1} = (2P + 1)\frac{\lambda_0}{4} \tag{3}$$

$$l_{t2} = (2Q + 1)\frac{\lambda_0}{4} + 2\Delta L \tag{4}$$

$$W_{t1} = \frac{7.475h}{e^x} - 1.25t \tag{5}$$

$$x = \frac{Z_0\sqrt{1.41 + \epsilon_r}}{87} \tag{6}$$

$$Z_0 = \sqrt{50 \times \frac{11.96\lambda_0}{W}} \tag{7}$$

where, P and Q are non-negative integer numbers (here, $P = Q = 1$).

Series-fed array structure is chosen to achieve a high gain antenna profile at the cost of a little bit increased layout area. Further, the directive gain can be enhanced remarkably by placing parasitic patch structures at the non-radiating edges of the main radiating elements. Effectively, the aperture size of the whole planar array antenna is enhanced, which further causes an increase in gain. The gap between the primary antenna and parasitic patch decides the amount of E-field coupling. To ensure strong coupling and optimal excitation of the parasitic patch element, its gap 'g' from the main radiating element should be minimum. Systematic parametric studies have been carried out to get an optimum value of gap 'g' and width of parasitic patch 'W_p' and are indicated in the S_{11} plot of Fig. 2. As can be noted from the plot of Fig. 2b, for a gap dimension of 50 to 200 μm, there is hardly any difference in resonant frequency, but a slight change is observed in the refection coefficient curve. Actually, the flux linkage phenomenon is not captured clearly with the results. But, when the width of parasitic patches 'W_p' is changed, it changes the impedance and current vector of the antenna. The dimension of all the design parameters has been optimized and summarized in Table 1. The surface current distribution of this enhanced gain RMAA is depicted in Fig. 3. As revealed from the plot, the energy associated with each patch element monotonically decreases from the directly fed array element to the last element. This is because most of the energy is radiated by

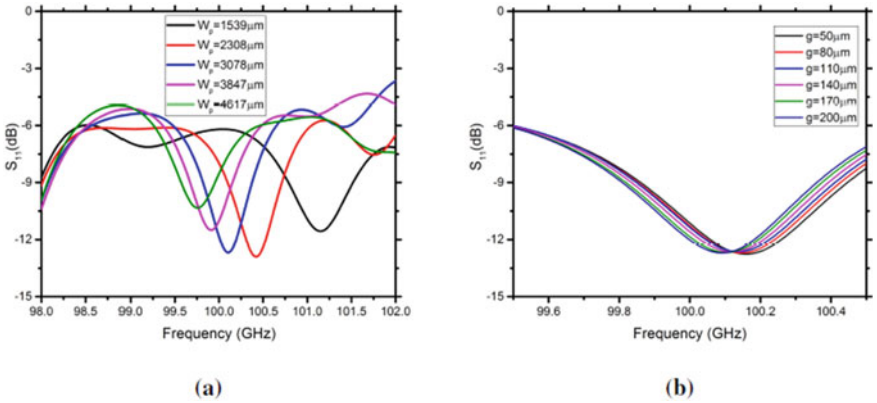

Fig. 2 Variation in reflection coefficient of parasitic patch loaded RMAA with **a** width of the parasitic patch **b** gap between the main and parasitic patch element

Table 1 Optimized dimensions of the RMAA with parasitic patches

Parameter	Values (in μm)
W	3078
L	2489
l_{t1}	1293
l_{t2}	2685
W_{t1}	500
W_p	1539
g	200
h	100

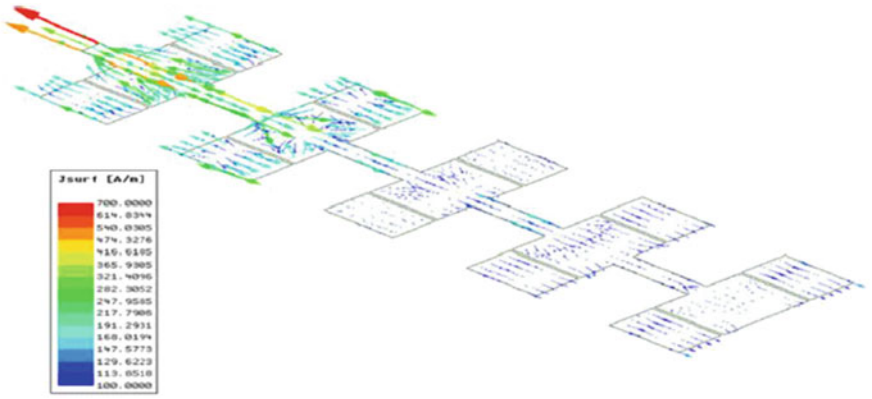

Fig. 3 Surface current distribution for RMAA structure

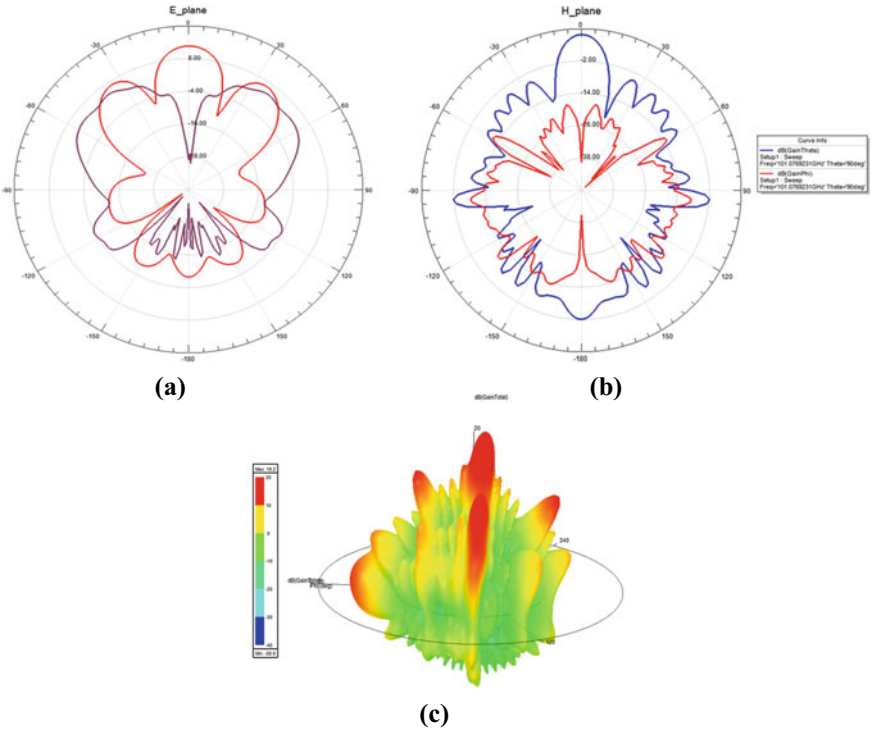

Fig. 4 Simulated far-field radiation patterns for RMAA at 100 GHz in **a** E-plane; **b** H-plane; **c** 3D-plot of the radiation pattern

the first patch itself, and the remaining is passed to the next patch, which radiates the partial amount of energy and partially transfers it to the next.

Simulated far-field radiation pattern of the antenna is shown in Fig. 4. H-plane indicates the broadside profile at the broadside direction and X-pol level is 38 dB below than Co-pol. E-plane pattern is like a flower with multi-shape petals. Peak simulated gain is obtained as 19dBi.

Another option of enhancing the gain of the RMAA structure is utilizing a superstrate structure instead of parasitic patch loading. Figure 5 demonstrates structural description of superstrate structure loaded antenna architecture with detailed cross-sectional and isometric views. Here, h_s is the height of the superstrate material, h_a is the height of air column and h_{sub} is the thickness of the substrate. In this composite structure, in practice, air column is realized by placing a honeycomb structure, whose electrical property greatly resembles air. It is a carbon fiber based material made by Ultracor Company which offers thermal stability of near zero CTE. Part number of the structure is UCF-126-3-8-2.0 [13]. Figure 6 shows the real honeycomb structure used for THz antenna realization.

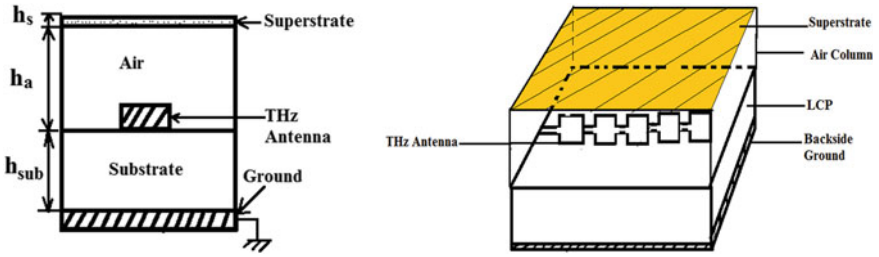

Fig. 5 Superstrate loaded THz antenna for gain enhancement in **a** cross-sectional view; **b** isometric view

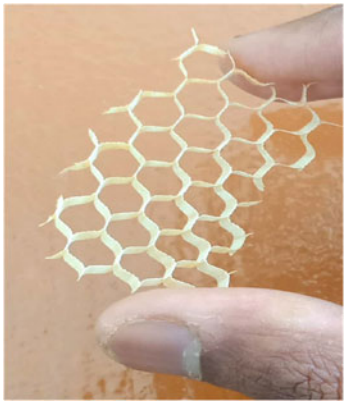

Fig. 6 Ultracor honeycomb structure (Part No. UCF-126-3-8-2.0)

This method works on the structural resonance method, and it is also known as the resonance gain method. Earlier, this method has been used to design load-bearing antenna structures [14]. The detailed analysis of this structure with the help of the transmission line model is done in [15]. Co-relation between the substrate thickness and superstrate height is obtained with respect to operating wavelength for a high gain antenna module. The position and thickness of the superstrate are the important parameters for exciting the structural resonance, leading to a higher gain of the whole antenna structure. Three different types of microwave materials are used as superstrate materials, such as-FR-4, quartz glass, and high resistive silicon. Two cases are studied to improve the gain of basic RMAA by the superstrate layer. In the first case, the position of the Silicon superstrate of thickness $h_s = 675$ μm is varied from 0.25 λ_0 to 1.5 λ_0. Corresponding *S*-parameters are shown in Fig. 7a. We can observe that for $f_0 = 100$ GHz; the resonance occurred for every 0.5 λ_0 step size starting from $h_a = 0.75$ mm. While in the second case, we have varied the superstrate material. The position and the thickness of each superstrate material are determined by the high gain curve for 100 GHz [15]. These dimensions are optimized and listed in Table 3. The *S* parameter performance for this case is shown in Fig. 7b, and we can observe that structure is resonating at desired 100 GHz frequency for all superstrate

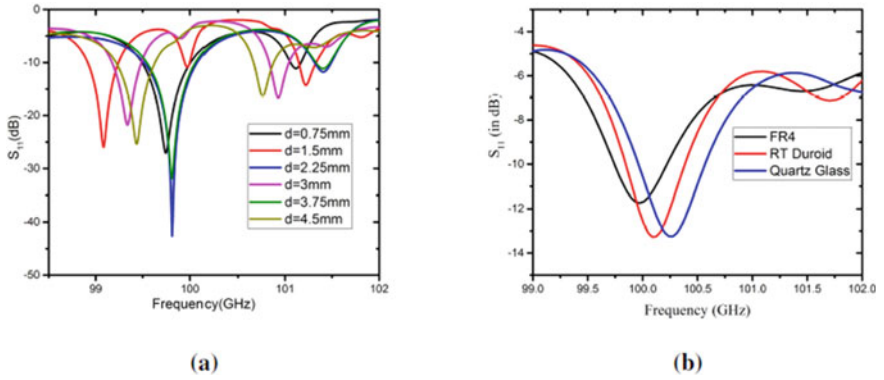

Fig. 7 S_{11} parameter for **a** silicon superstrate with different 'd' **b** different superstrate

layers. The 3D radiation patterns for different superstrates are shown in Fig. 8. It is observed that due to the superstrate, the gain is improved by 3 dB as compared to the stand-alone basic RMAA structure. It has also been observed from the FEM analysis that, the antenna with glass superstrate has very high cross-polarization in H-plane, as shown in Fig. 9 (Table 2).

2.2 Sectoral H-plane Horn Antenna

Horn antenna is a widely used simplest and robust candidate of engineers' choice from decades ago. Because of its several inherent characteristics, like wide bandwidth, stable radiation pattern, etc. its demand in the antenna world still remains unaltered as compared to its counterparts. Like lower frequency gamut of EM spectrum, horn antenna becomes indispensable for realizing the feeding network or as a combiner in monopulse tracking radar even in THz frequency bands. It drives the engineers to develop an efficient way of manufacturing such antennas out of advanced fabrication methodologies.

Literature reveals that, one such promising technology in 'Silicon micromachinng' [16–18]. Implementing DRIE (Deep Reactive Ion Etching) method along with wafer bonding makes it possible to realize. Here, in this chapter, we discuss such a silicon micro-machined *H*-plane sectoral horn antenna. Two different frequency bands (75 to 110 GHz and 220–330 GHz) have been targeted here for a 13 dBi gain horn antenna. Flaring the dimension of rectangular waveguide in direction of *H*-field keeping other dimension constant forms *H*-plane sectoral horn. It is expected that, radiation patterns in *H*-plane will be much narrower than *E*-plane because of flaring and larger dimension is in that direction. Design of this horn, as explained in the following subsection, is systematically accomplished using 'normalized directivity v/s aperture size curve'. The directivity and aperture size are related as follows [19]:

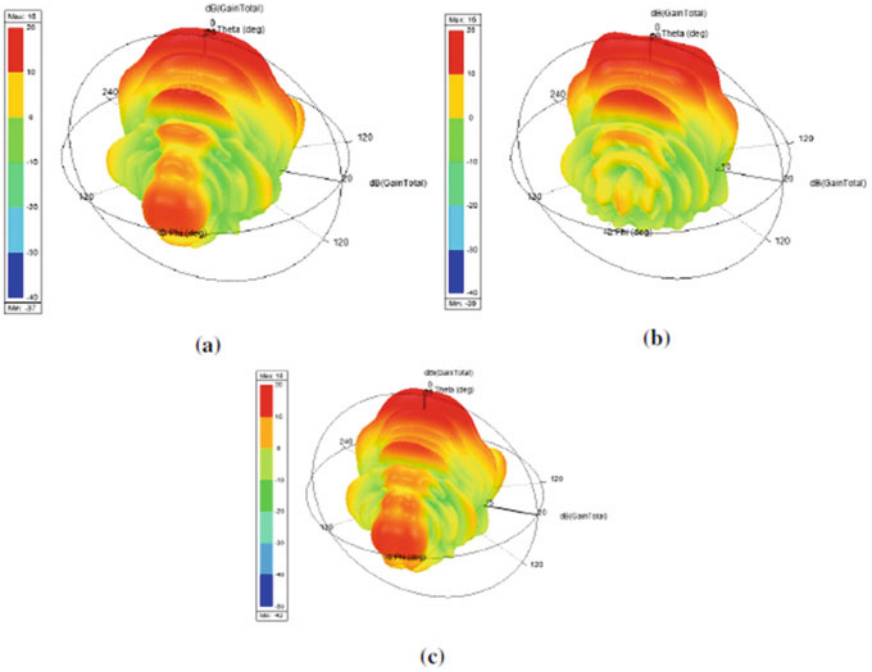

Fig. 8 3D far-field pattern for **a** RT duroid superstrate **b** Quartz glass superstrate **c** FR4 epoxy superstrate

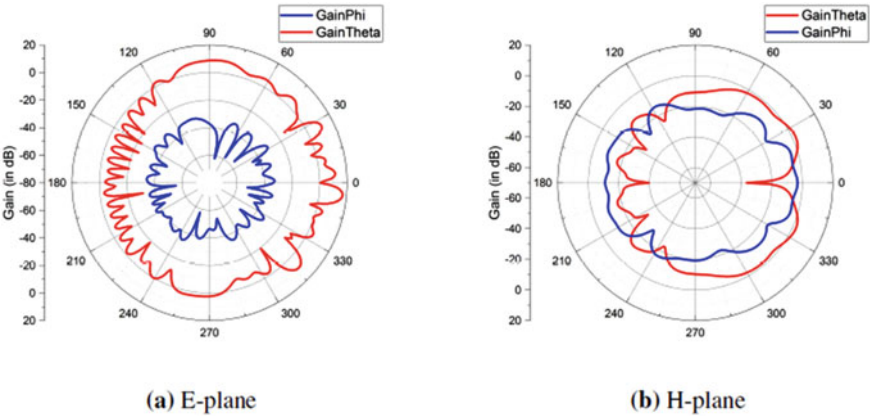

Fig. 9 Co-pol and X-pol levels in principle planes for glass superstrate RMAA

Table 2 Optimized dimensions of the RMAA with superstrate

Parameter	Values (inμm)
W	3078
L	2489
$^{l}t1$	1293
$^{l}t2$	2685
$^{W}t1$	690

Table 3 Dimension of the composite antenna array with superstrate materials

Superstrate material	Thickness, h_s (in mm)	Height of air column, h_a (in mm)
RT duriod	0.51	1.5
FR4 epoxy	0.35	1.5
Quartz glass	0.55	1.5

$$D_H = \frac{b}{\lambda}\frac{G_H}{\sqrt{\frac{50}{\lambda\rho_h}}} \tag{8}$$

where, 'D_H' is the directivity for H-plane horn antenna, 'b' is the height of the rectangular waveguide, 'λ' is the operating wavelength, 'a' is the width of the feeder waveguide, 'a_1' is the flaring width of the horn antenna, and 'ρ_h' is hypotenuse of right angle triangle form in H-plane given by Eq. (9) and (10).

$$\rho_h = \sqrt{\rho_2^2 + \left(\frac{a_1}{2}\right)^2} \tag{9}$$

$$G_H = \frac{32}{\pi}\frac{a_1}{\lambda}\sqrt{\frac{50}{\lambda\rho_h}} \tag{10}$$

H-plane sectoral horn is designed using flowing steps:

- Defining the desired gain (if it is in dBi convert it to absolute value) of horn antenna.
- Finding the corresponding optimum ρ_1 from the standard normalized directivity versus aperture size graph for H-plane sectoral horn antenna.
- The aperture size a_1 is correspondingly obtained from optimum ρ_1 value.

Using above mentioned steps the 13 dBi, WR-10, and WR-3.4 Waveguide based H-plane horn antenna is designed and simulated. Figures 10 and 11 show the schematic diagram of the proposed horn. The optimized dimension of antenna structure is given in Table 4. The S-parameter performance is shown in Fig. 12. As revealed from the plot, the S_{11} is below -10 dB in the desired band. Figures 13 and 14 show the far-field plots for these antennas in the principle plane. As it can be observed

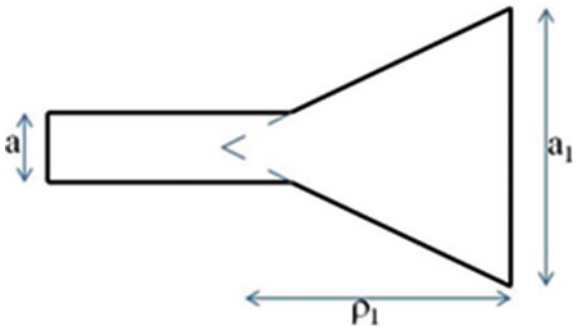

Fig. 10 H-plane view of horn antenna

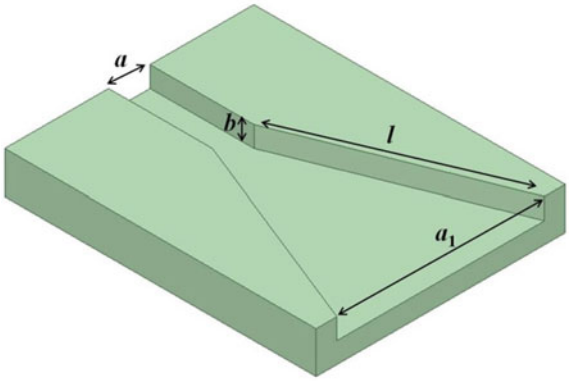

Fig. 11 Isometric view of *H*-plane horn structure

Table 4 Optimized dimensions of the *H*-plane horn antenna

Parameter	WR-10 based structure (in mm)	WR-3.4 based structure (in mm)
a	2.54	0.864
b	1.27	0.432
l	34.63	14.85
a_1	20.12	7.3

that, the *H*-plane plot is much narrower than *E*-plane plot and has simulated gain of 13 dBi. Thus simulated results have close relevance to theory. In addition to this, *X*-pol level is 37 dB below the Co-pol level in principle.

3 Circuit Modeling of THz Antenna

Equivalent circuit model is used for representing the antenna impedance. This helps in extracting features of the antenna. An RLC resonator model has been widely used in modeling antenna impedance. Similar model is attempted here. Out of two antenna categories, circuit modeling for complicated array structure is tried out here.

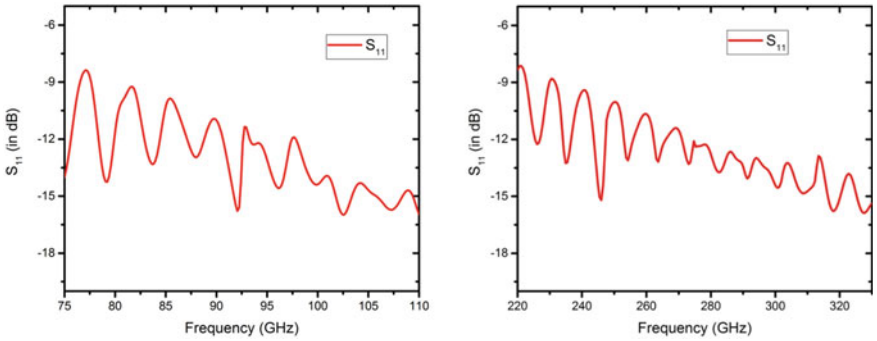

Fig. 12 S_{11} Parameter for **a** WR-10 waveguide based **b** WR-3.4 waveguide based *H*-plane horn structure

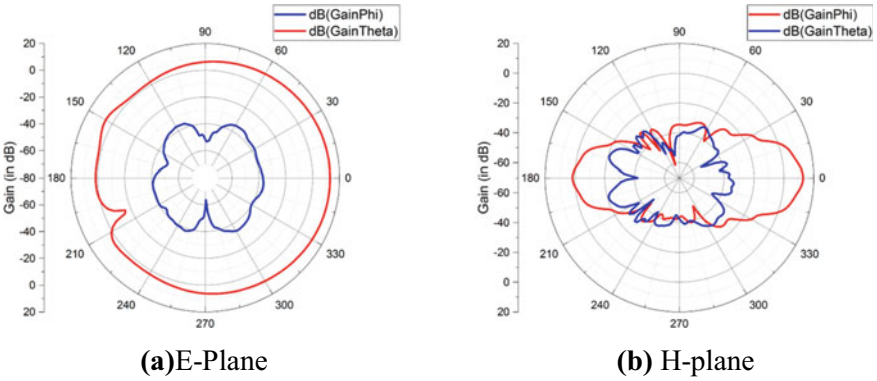

Fig. 13 Far-field pattern for WR-10 based *H*-plane sectoral horn

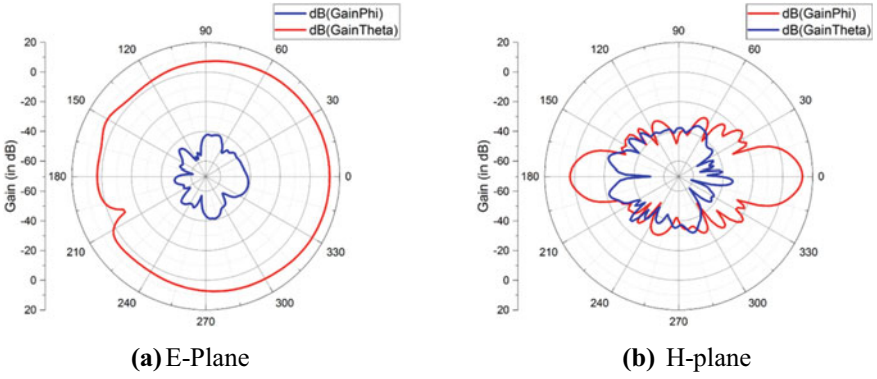

Fig. 14 Far-field pattern for WR-3.4 based *H*-plane sectoral horn

The proposed array structure consists of five main radiating elements, transmission line segments in between them, ten parasitic patches, and feed line as shown in Fig. 15. Main radiating elements are represented by lossy tank circuit (L_{10}; R_{10} and C_{10}) corresponding to TM_{10} mode. Feeding network is represented by series combination of L_f and R_f due to finite conductivity of metal used. Parasitic patches are nothing but capacitive or dielectric loading depending upon substrate electrical properties. Hence, it can be modeled as a leaky capacitor. Transmission line segments between the patches are represented by a combination of lossy inductor and capacitor, corresponding to the parasitic capacitance effects. This lumped circuit is simulated in ADS and tuned to 100 GHz. The obtained lumped components values are listed in Table 5. The S_{11} parameter from lumped circuit and RMAA structure is shown in Fig. 16.

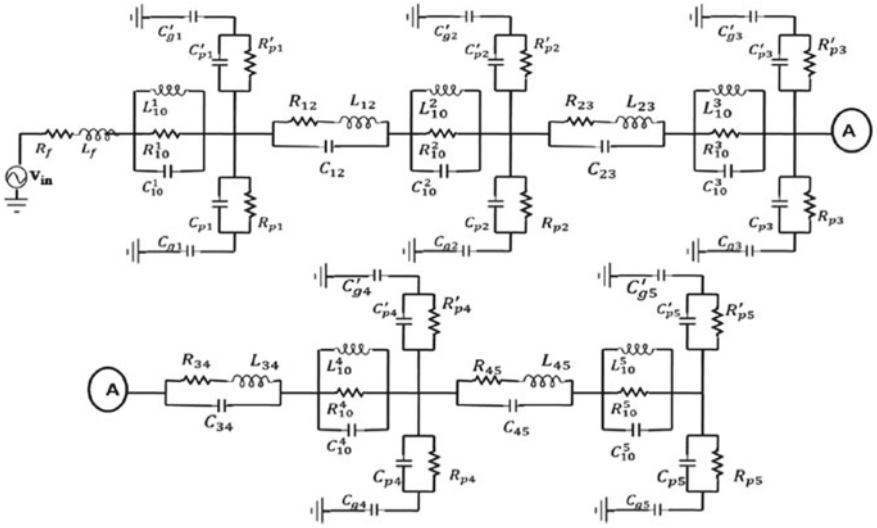

Fig. 15 Transmission line model for the RMAA with parasitic patches

Table 5 Lumped components values for a simulated equivalent model

Variables	Values	Variables	Values
R_f	0.01Ω	R_f	161.12Ω
L_f	54pH	^{C}gi	16.45pF
L^i_{10}	4.28pH	C_pi	16.45pF
R^i_{10}	44Ω	^{R}ij	55.56Ω
C^i_{10}	0.591pF	^{R}pi	161.12Ω
C^i_{gi}	16.45pF	^{L}ij	1100pH
C^i_{pi}	16.45pF	C^i_{ij}	7.4pF

Note i varies from 1 to 5 and $j = i + 1$ varies from 2 to 5

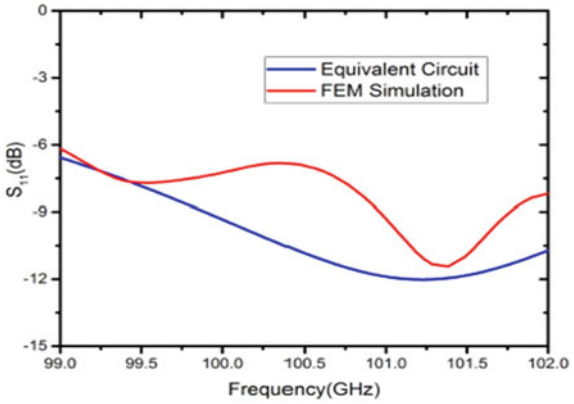

Fig. 16 S_{11} comparison of T-RMAA with parasitic patches and equivalent model

4 Fabrication of Prototypes

Two prototype structures of microstrip patch antenna array have been fabricated on 4 mil thick Liquid Crystal Polymer ($\epsilon_r = 3.14$, $\tan\delta = 0.002$) substrate. Figure 17 shows the fabricated prototypes (front view), explaining the flexibility of substrate. Standard wet etching chemistry has been used to pattern the metal layer (25 μm of copper). The backside of the substrate is fully metalized to realize the common ground plane. Currently, the testing process of these antennas is in progress.

The fabrication steps for horn antenna are schematically explained in Figs. 18 and 19. The steps can be described as follows:

(i) It is two wafer processes. Initially, two double-side polished silicon wafers are taken and given requisite chemical cleaning (RCA + SPM) to eliminate

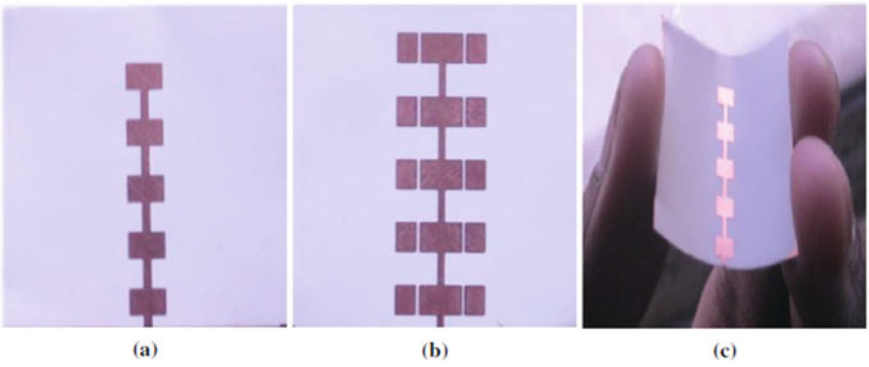

Fig. 17 Fabricated prototypes of the **a** antenna array **b** array with parasitic patches **c** illustration of the conformal shaped antenna

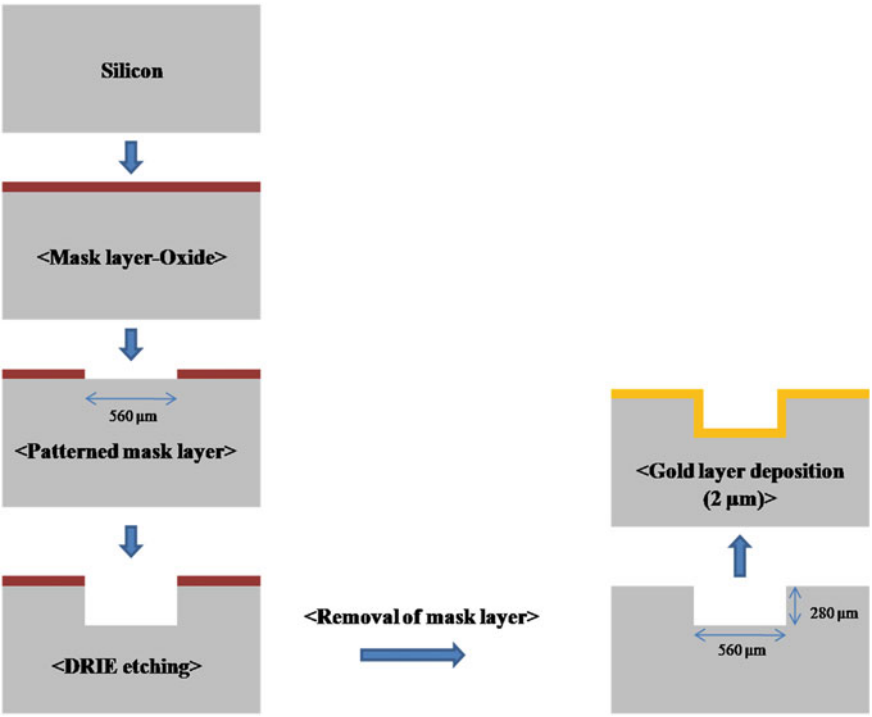

Fig. 18 Preparation of first silicon wafer for making the horn antenna

all possible organic and inorganic contaminants. After that, on the first wafer following process steps have been performed:

(a) A thick oxide layer is deposited on its front side.
(b) The oxide layer is patterned to form a channel through DRIE etching.
(c) DRIE process is applied up to the depth of lateral dimension of the rectangular waveguide.
(d) Oxide layer is removed.
(e) A conformal gold layer is evaporated to metalize the trench.

(ii) Whereas, on the second wafer gold is deposited on the front-side by E-beam evaporation.

(iii) Second wafer is flipped to make the metal layer at its bottom side, and then both of the wafers are bonded together adopting the Eutectic bonding at 363˚C. Thus the waveguide channel is formed.

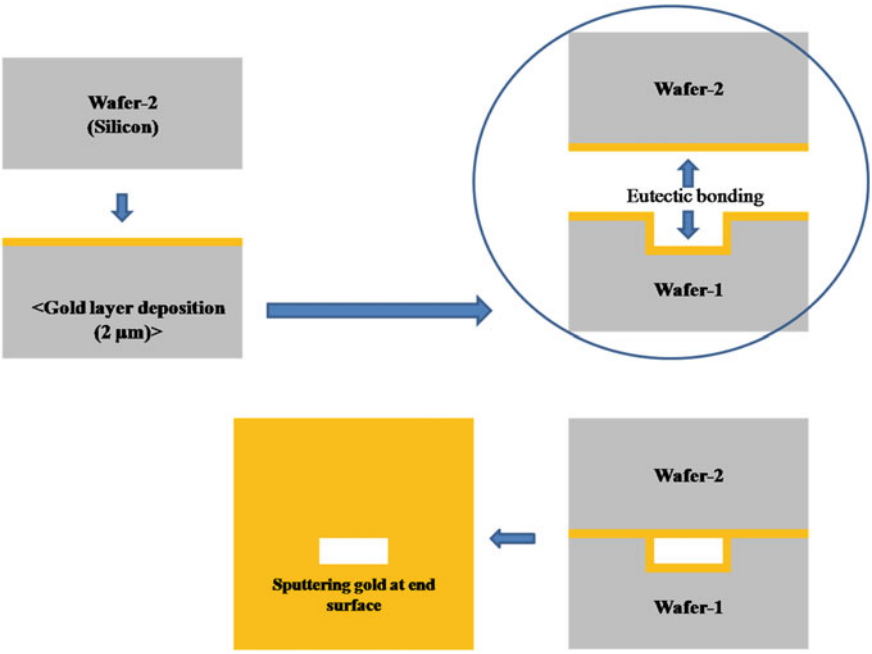

Fig. 19 Generic fabrication steps of horn antenna realization implementing silicon micromachining technique

5 Conclusion

This chapter highlights the essence of high gain antenna module for communication systems in Terahertz regime. Two different types of antennas (horn antenna and microstrip patch array) have been discussed with planar geometries. Ease of design and fabrication simplicity is the main attractive features of these antennas. Detailed design along with circuit modeling and fabrication process details have been covered in this chapter. Parametric simulations were carried out to explore the optimum design parameters. One of the antennas is demonstrated over a bio-compatible, flexible type substrate at 100 GHz, which can further be utilized for medical imaging applications. Effect of superstrate structure is efficiently implemented to enhance the gain of the planar antennas. Another structure involves silicon micromachining technology, where DRIE is extensively used in two silicon wafers separately. Finally, to get an integrated module, two such wafers are bonded. Real time testing of the antenna is underway.

References

1. Z.D. Taylor et al., THz medical imaging: in vivo hydration sensing. IEEE Trans. Terahertz Sci. Technol. **1**(1), 201–219 (2011)
2. D.M. Mittleman et al., Recent advances in terahertz imaging. Appl. Phys. B **68**(6), 1085–1094 (1999)
3. Fukunaga et al., Terahertz spectroscopy applied to the analysis of artists' materials. Appl. Phys. A **100**, 591–597 (2010)
4. C.M. Armstrong, The truth about terahertz. IEEE Spectr. **49**(9), 36–41 (2012)
5. T.G. Phillips, J. Keene, Sub-millimeter astronomy (heterodyne spectroscopy). Proc. IEEE **80**(11), 1662–1678 (1992)
6. M. Rahaman et al., THz communication technology in India present and future. Defense Sci. J. **69**(5), 510–516 (2019)
7. G. Chattopadhyay et al., Terahertz antennas and feeds, in *Aperture Antennas for Millimeter and Sub-Millimeter Wave Applications*. ed. by A. Boriskin, R. Sauleau (Springer International Publishing, Cham, 2018), pp. 335–386
8. N. Kingsley, "Liquid crystal polymer: enabling next-generation conformal and multilayer electronics". Microw. J. 188–200 (May 2008)
9. D.C. Thompson, O. Tantot, H. Jallageas, G.E. Ponchak, M.M. Tentzeris, J. Papapolymerou, "Characterization of liquid crystal polymer(LCP) material and transmission lines on LCP substrates from 30 to 110 GHz". IEEE Trans. Microw. Theory Tech. **52**(4), 1343–1352 (April 2004)
10. Georgia Tech Report. Available: https://phys.org/news/2006-08-georgia-tech-liquid-crystal-polymer.html
11. C.A. Balanis, "*Antenna Theory Analysis and Design*", 3rd edn. (Wiley, 2005)
12. M.S. Rabbani, H. Gi-Shiraz, "Improvement of microstrip antenna's gain, bandwidth and fabrication tolerance at terahertz frequency bands". *Processing Wideband Multi-Band Antennas Arrays Civil, Security Military Applications Conference* (2015)
13. www.ultracorinc.com
14. C.S. You, W. Hwang, S.Y. Eom, "Design and fabrication of composite smart structures for communication, using the structural resonance of radiated field." *Smart Materials and Structures*, 14.2 (Mar. 2005), pp. 441–448
15. C. You, M.M. Tentzeris, W. Hwang, Multilayer effects on microstrip antennas for their integration with mechanical structures. IEEE Trans. Antennas Propag. **55**(4), 1051–1058 (2007)
16. G.M. Rebeiz, "*RF MEMS Theory, Design, and Technology*". (Wiley, 2003)
17. J. Iannacci, RF-MEMS for high-performance and widely reconfigurable passive components—a review with focus on future telecommunications, internet of things (IoT) and 5G applications. J. King Saud Univ.-Sci. **29**(4), 436–443 (2017)
18. A. Karmakar, K. Singh, *"Si-RF Technology", ISBN: 978-981-13-8051-8*, 1st edn. (Springer, Singapore, 2019)
19. L. Jun, A universal method for directivity synthesis. IEEE Trans. Antennas Propag. **35**(11), 1199–1205 (1987). https://doi.org/10.1109/TAP.1987.1144014

Element Failure Correction Techniques for Phased Array Antennas in Future Terahertz Communication Systems

Hina Munsif, B. D. Braaten, and Irfanullah

Abstract The terahertz frequency band is the range of frequencies from 300 GHz to 10 THz (above the microwave range and below the optical spectrum) in the electromagnetic spectrum. The future terahertz-range indoor communication system will require a highly directive terahertz beamforming antenna array to switch between different devices (mobile, home appliances, etc.). As such, there will be a high probability of antenna elements failure, which will disrupt the high-volume wireless communications. Therefore, study and analysis of antenna array failure correction techniques are important. In the literature, only a few methods have been reported for array element failure correction. This chapter provides an overview and tutorial on the methods that have been reported in the literature for array element failure correction in the context of terahertz beam control. A pattern recovery technique of low sidelobe antenna arrays operating at 3.5 THz, using the iterative Fourier technique (IFT) is discussed. The occurrence of defective elements across the array is included by setting the associated excitation coefficients to zero. The presented results are related to 1×8 linear patch antenna array failure correction model with half-wavelength inter-element spacing operating at 3.5 THz in MATLAB and CST simulators. The array failure correction using this method is evaluated for various sidelobe levels (SLLs), where the failed elements are randomly dispersed across the array. The analysis of array failure correction algorithm on the sidelobe level (SLL), directivity, half-power beamwidth (HPBW), and taper efficiency of the recovered radiation patterns are reported in detail, and guidelines are provided on the performance parameters.

Keywords Phased arrays · Radiation pattern · Optimization · Microstrip arrays

H. Munsif · Irfanullah (✉)
Electrical and Computer Engineering Department, COMSATS University Islamabad, Abbottabad, Pakistan
e-mail: eengr@cuiatd.edu.pk

B. D. Braaten
Electrical and Computer Engineering Department, North Dakota State University, Fargo, USA

S. Das et al. (eds.), *Advances in Terahertz Technology and Its Applications*,
https://doi.org/10.1007/978-981-16-5731-3_2

1 Introduction

The antenna is the main component in wireless communication, which was first revealed by Marconi in 1901 [1–3]. Terahertz (THz) frequency band (0.3 THz to 10 THz) is a part of sub-millimeter EM (electromagnetic) spectrum, shown in Fig. 1a. Recently in wireless communication, the terahertz frequency band has been reserved for real life applications [4], as shown in Fig. 1b. In the literature, recently there is growing research on THz applications, for example in communications, sensors, radar, imaging, and other research applications [5–7]. Some of the major reasons for the increasing interest in THz frequency band are given below [8, 9]:

1. THz radiations are able to penetrate through luggage and covering materials like corrugated cardboard, packaging, book bags, clothes, and shoes, etc. to discover any dangerous or unsafe materials concealed within.
2. The THz systems do not damage the suspect or human body that is scanned under THz radiations.
3. Terahertz imaging systems can detect corrosion or deterioration on metallic exterior of aerospace structure and any fault in composite materials of aerospace structure as well [10, 11].
4. The ECRs imaging and terahertz spectroscopy have been explored intensively for possible biomedical, security, and defense applications.

As antenna is the backbone for every wireless application and therefore antenna arrays are used for the purpose of beamforming and increasing the gain of antenna. Usually, the antenna arrays are made of large number of antenna elements. Hence, there is a high probability of failure of radiating elements. Phased antenna arrays used for radar and satellite applications can have element failure typically due to amplifiers. As antenna arrays are used in battlefield, aerospace, and other communication applications, so the damaged components in antenna arrays are hard to be repaired in real time. The failure of radiating elements can result in an increase in sidelobe level (SLL), filling nulls position, beam widening, and loss in gain, depending on the number of failed elements. To recover these performance parameters of array

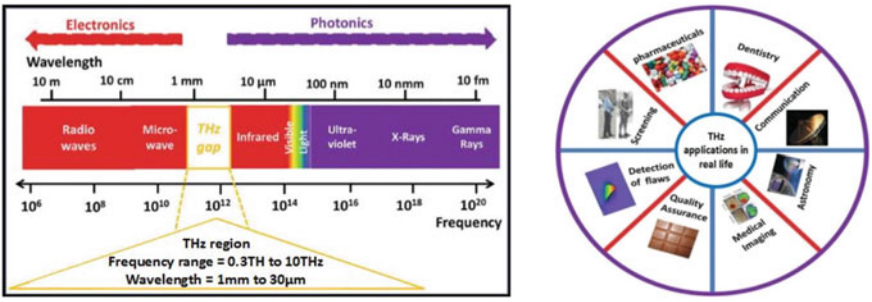

Fig. 1 THz frequency **a** Frequency range and wavelength **b** Applications in real life

by replacing non-radiating elements is quite impossible in situations, where antenna array is on a platform in space. The hardware replacement is a costly way to recover the array availability. While the presence of faulty elements makes antenna array non-symmetrical, because of this issue, the traditional analytical techniques are difficult to implement. Recently, the researchers have explored some self-repairing techniques based on optimization and these optimization techniques can recover the array pattern in the presence of failed elements. Thus, researchers sort out an approach through which the properties of array radiation patterns can be maintained: this approach is to re-synthesize or recalculate the excitation coefficients of the working elements instead of replacing them. In the literature, there are two approaches for antenna array failure correction: (1) software solutions: some of them are optimization algorithms, for example, PSO (particle swarm optimization algorithm), GA (genetic algorithm), BFO (bacteria foraging algorithm), and IFT (iterative Fourier technique), and (2) hardware solutions: rarely used due to its complicated designs (discussed in section I.II).

1.1 Antenna Array Failure Correction Software Techniques

In the software techniques presented in this section, majority algorithms work to recalculate the amplitudes/phases of the array antenna elements for radiation pattern recovery. In [12], the proposed algorithm calculates the new phases of non-defective phase shifters to restore the broad null (20° to 30°) with −66 dB depth in the desired direction of the 28 isotropic elements linear array pattern. It is shown that the null can be recovered at the cost of increasing SLL for random elements failures. A rectangular 5800 elements planar array was investigated in [13] for SLL (−45 dB) and gain by defecting 290 random elements using inverse Fourier transform. In [14], 50 and 80 elements linear isotropic array was investigated for low SLL (−45 dB) synthesis using 8 elements random failure. In [15], the genetic algorithm (GA) can recover the best pattern with SLL of −20 dB for 18 and 44 elements linear isotropic arrays from the damaged pattern by re-synthesizing the excitation for the working elements. The work in [16] has presented a novel real-time pattern correction approach based on sparse-recovery technique on 17 × 17 planar arrays for SLLs of −20 dB and −40 dB. The IFFT approach in [17] has investigated single and dual wide nulls along with specified SLL value for 1 × 34 linear isotropic arrays. The DE (Differential Evolution) algorithm in [18] is used to investigate the 1 × 30 linear half-wave dipole array by optimizing spacing among antenna elements for pattern recovery in case of antenna elements failure. In [19], the performance of two optimization algorithms particle swarm optimization (PSO) and bacteria foraging optimization (BFO) is analyzed. By using the above algorithms, the excitations were recalculated for the array with elements failure and the radiation patterns are restored. The main emphasis of [19] was to recover the SLL and steering nulls in the specified directions, using amplitude correction approach. The analysis was performed on a 1 × 32 linear array with element spacing of λ/2, and the array was designed at 2.33 GHz. The